Integrity Management of the Reachable Space With Lane Grid Maps

Corentin Sanchez, Philippe Xu, Philippe Bonnifait, Alexandre Armand

Integrity Management of the Reachable Space with Lane Grid Maps

Corentin Sanchez*, Philippe Xu*, Philippe Bonnifait*, Alexandre Armand**

***Abstract*—For an autonomous vehicle, reliable situation understanding is a key component of safe navigation. An incorrect prediction of an upcoming situation means that erroneous information may be supplied to the decision-making process, leading to hazardous outcomes. It is therefore of great importance to estimate the driving areas that are reachable by other interacting road users, without introducing misleading information. This paper presents a means of handling the integrity of prediction information, given the imperfection of object prediction, via a Lane Grid Map, that is to say a spatial representation of the situation at a tactical level, based on the topological layer of a high-definition map. We demonstrate experimentally, using real data, how the spatial sampling step of the grid representation can be used to manage the integrity of prediction information. Moreover, addressing interactions during the prediction makes it possible to handle some particular situations safely. We show how some interactions can be utilized via the concept of neutralization. To quantify the integrity of the prediction, we propose the use of two metrics, namely False Negative Rate and Neutralized Time Interval. Experiments were carried out with three vehicles to evaluate the integrity of the prediction using these metrics.**

***Index Terms*—Situation understanding, prediction of driving situations, integrity of navigation information**

I. Introduction

ONCE an autonomous vehicle navigating on open roads has its own representation of the current situation, it needs to obtain a prediction of what is going to happen subsequently, which is the highest level of situation understanding. Usually, prediction is concerned with the most likely situation that the vehicle is about to encounter, and is part of a situation awareness strategy [1]. Prediction enables actions to be planned via decision-making processes. A large number of works have been undertaken in this area. Decision planning and prediction can be done at different levels of abstraction [2]. In the present work we focus on prediction over a period of a few seconds at the maneuver level, also known as the tactical level. Prediction must be done without compromising safety, as the likelihood of unexpected behaviors increases as time goes by.

A key issue in prediction is providing reliable information over the relevant time horizon. A misunderstanding of the situation can result in behaviors that are hazardous. Preventing misunderstandings of this kind depends partly on ensuring that the navigation information provided to the decision and control systems is not misleading, and a considerable amount of work in this area is to be found in the literature [3] [4]. The key concept here is *integrity*, which has been extensively studied for GNSS systems [5], and is a concept that has also been applied to certain other problems including lane-level map-matching [6]. In this paper, the core of our methodological approach involves extending this concept of integrity to the information encoded in a grid-based representation. To set the scene, let us consider an example of misleading information. Fig. 1.a shows a situation from the point of view of the blue vehicle at the current time t_0. This representation has been produced by the blue vehicle itself using its own exteroceptive sensors, a localization system and an High-Definition (HD) map. The true position of the observed yellow vehicle is contained within the occupied cells in red. A prediction module computes the reachable bounds of the yellow vehicle and the corresponding reachable cells at some future time $t_0 + \Delta t$. In Fig. 1b, the predicted bounds are incorrect, since the true future position of the yellow vehicle is no longer fully within the bounds. The incorrect bounds prediction may have a variety of causes, and in this particular case it may be caused by an underestimation of speed. Here we have an incorrect prediction that could potentially lead to a hazardous situation, since the ego vehicle may consider wrongly that it has time to turn right in front of the yellow vehicle.

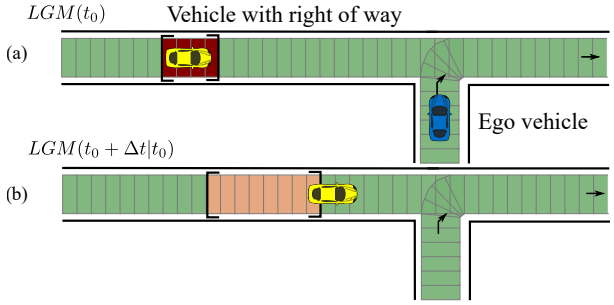

Fig. 1: At the current time t_0, the ego vehicle has a grid-based representation of the situation with free (green) and occupied (red) spaces (a). To turn right, it needs to predict the evolution of the situation at a future time $t_0 + \Delta t$. In situation (b), the prediction is misleading as the true position of the yellow vehicle is outside of the bounds of the reachable orange area.

Our methodology adheres to the outline shown in Fig. 2. We use the formalism of Lane Grid Maps (LGMs), introduced in [7]. A geometric model of this kind is well suited to formal safe decision methods such as that presented in [8]. In addition, the integrity of the information it contains can be managed, and consequently the decision and control methods of the vehicle are not at risk of being misled.

* Are with Université de Technologie de Compiègne, CNRS UMR 7253 Heudiasyc, 60200 Compiègne, France.
** Is with Renault S.A.S, Guyancourt, France.

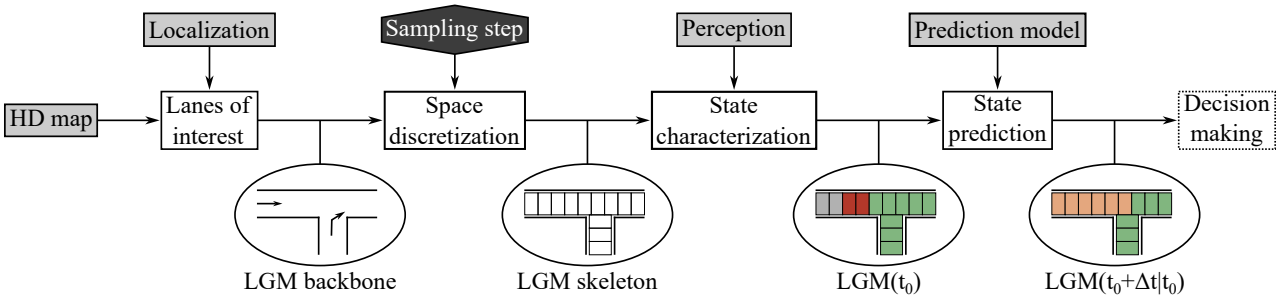

Fig. 2: LGM computation and prediction diagram. Grey boxes are inputs. The white boxes are the different steps to build the LGM and its prediction. The sampling step, which is a key parameter of the LGM integrity, is depicted in black.

The methodological contribution of our paper is threefold. First, the concept of integrity is formalized within a grid-based representation of the driving situation. More specifically, we introduce integrity metrics in terms of spatial occupancy and show that this integrity can be managed by tuning a spatial sampling parameter. Second, we extend the concept of integrity to situation prediction, where we quantify integrity in terms of spatial reachability. Third, the representation is enriched by taking into account physical interactions among road users, and we show that the same sampling step tuning process still satisfies the integrity constraint. All the methodological contributions were validated empirically via real experiments in the city of Compiègne, France.

The paper is organized as follows. Section II is devoted to related work, and we present different lane-level spatial representations and prediction methods that have been used in the literature. The three contributions listed in the previous paragraph are then detailed in three distinct sections, as follows. First, section III presents the LGM representation covering the computation of the lanes of interest, the discretization process and the characterization of cells. The integrity of the LGM information is formalized. Experimental results are presented to show how LGM integrity can be managed using the sampling step parameter. Second, in section IV, we extend the integrity concept to the reachability analysis of predicted LGMs. Third, section V proposes an enrichment of situation understanding via the concept of "Lane Neutralization", induced by physical interactions among road users. Experimental results are presented within the different sections.

II. Related work

A. World modelling

The literature features various architectures that seek to set up a so-called *world* or *context model* [9]–[11]. In [11], a distinction is made between scene representation from context modelling and situation representation from a planning point of view (defined earlier in [12]). In [9], the environment model, together with the situation analysis and prediction are instead part of the perception module.

Given a module that stores a world model, a situation can have several abstraction levels in terms of information and comprehension mechanisms. The three levels of abstraction identified some years ago in [13] are those also used in [11]. Among these, the Operational Level is the lowest level, offering a fine resolution of the space that provides a fine metric representation of the vehicle surroundings, and this can be used for short-term prediction. The Tactical Level is the intermediate level. It corresponds to a lane level, and the prediction of a situation at this level is on a longer time horizon (e.g. maneuvers). Finally, the highest level is the Strategic Level, having the most abstracted view of information. The Strategic Level offers a resolution of several hundred meters, and provides what is essentially a symbolic representation of the environment. At this level the mission planner, for example, plans a global trajectory over a wide space and time horizon.

The present research focuses on the tactical level, i.e. the lane level: the vehicle is aware of topological map information, and prediction at this level incorporates interactions. Two types of information can be distinguished, via object and spatial representations respectively. However, there is a need to combine these two different types of representation, as highlighted in the architectures presented in [9] and [14].

B. Spatial representations

Occupancy grid maps are probably the most popular discretized representation of environments, not least because they can be used for localization, planning, and tracking, as well as navigation [15], [16]. In general, the state of cells is defined by a distribution over the possible state values. Most of the time, the state of a cell is either free or occupied [17]. For automotive applications, cells can be characterized as drivable and not drivable as proposed in [18], or by risk metrics as in [19].

Parametric free space maps [20], created by combining parametric curves and geometric primitives, have been proposed to encompass the free drivable space. Uncertainties on the system inputs can be taken into account, giving rise to probability distributions corresponding to different parameters. The advantage of this approach is the compactness of the generated data. However, this approach, since it does not explicitly deal with *objects*, makes prediction operations more difficult.

C. Set-based prediction

There are several survey articles on motion prediction, including, for example, [21] and [22]. Prediction methods may

be separated into different categories relating to the operational or tactical levels. These methods may or may not take into consideration interactions at the strategic level.

A spatial representation that is able to handle occlusions and objects is needed for tasks like decision-making, but also for risk analysis [23] and safety evaluation [24]. In [25], set-based prediction is used in predicting the path and intention of a hypothetical road user that may potentially be hidden in an occluded area. Particle filters have also been used in determining the plausibility of a hidden road user [26].

Set-based prediction is also presented in [27] in the context of the SPOT project, where reachable areas of independent vehicles, known as reachable sets, are computed. For a given time horizon, the space that may be occupied by each vehicle during this interval is computed. In order to take into account interactions between road users, an intersection of different reachable sets can be performed by adding constraints, thus refining the reachability analysis strategy. Reachable space is bounded by the road layout as indicated by topological information, and computations are subject to some constraints [28]. For instance, a negative speed is not allowed, since vehicles always go forwards. When a vehicle cannot overtake a vehicle on a single lane, its prediction must remain consistent. There are several articles based on reachable sets that have given rise to further work, e.g. in trajectory planning [29].

D. Positioning of the approach

In this paper we propose a world model based on a discrete representation of the navigable space guided by an HD map. This approach seeks to leverage the advantages of existing approaches while providing integrity control mechanisms at a tactical level. Integrity is addressed both in real time and in predicting reachable space, where some physical constraints among road users are taken into account. Our approach makes use of an LGM representation, as described in the next section.

III. Lane Grid Map: a lane-level representation

An LGM is an ego-centered spatial representation at a tactical level. It allows situation understanding in the areas of interest of the ego vehicle. The LGM focuses attention on areas whose relevance will be determined by the particular road network. A localization system is used to map-match the pose of the vehicle to a lane on a road. An Interaction Graph (IG) structures the areas of interest using an HD map [7]. The map is a graph structure with topological and metrical levels. The lanes in the map are represented by their center as a polyline with a high accuracy, and are connected through spatial relations, e.g. crossing or merging or adjacency. Additional information on the road infrastructure may also be available, such as lane width, traffic law priorities, and speed limits. Each node of the graph corresponds to a specific area. Fig. 3 shows the application of the IG representation. The lanes that the ego vehicle intends to follow are shown in blue. There are nodes corresponding to areas that are of high importance, called primary-order nodes, e.g. the red lanes that cross and merge with the blue lane, and others that are of secondary order, e.g. the orange lanes that have direct interactions with the red lane. In Fig. 3, only indirect interactions with respect to the merging lane in red are shown.

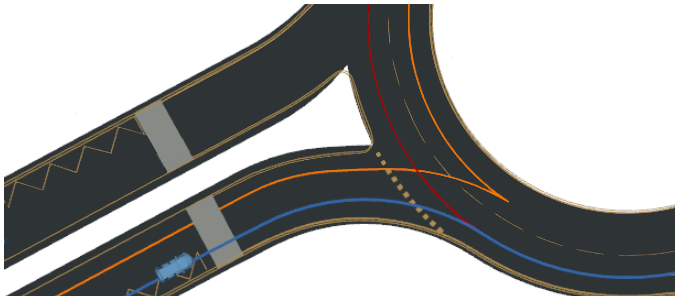

Fig. 3: Lanes of interest in a real experiment led in Compiègne. The ego vehicle is represented in blue and its intended path represented by the blue line. The red line represents lanes in direct interaction with the ego vehicle path and the orange lines are lanes that interact indirectly.

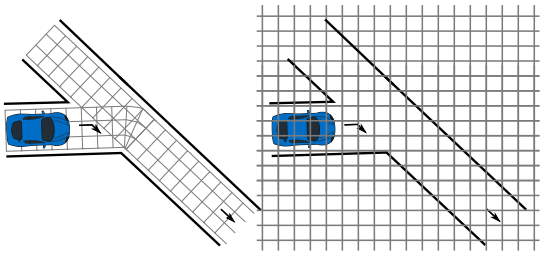

Fig. 4: Left: an LGM for a merging intersection. The ego vehicle (blue) intends to turn right. Right: A Cartesian OG.

The ego vehicle must focus on the space where it is likely to evolve and on the scene elements with which it may interact. The LGM lane-level representation is built upon the IG that focuses on areas of interest and serves as a backbone.

A. A lane-level space representation

At the lane level, the autonomous vehicle has to convert the topological information provided by the IG into a metrical representation. The proposed lane-level grid representation is a spatial grid based on a discretization of the lanes of interest along their longitudinal direction. Based on the geometric layer of an HD map, the lanes are discretized in successive contiguous quadrangles, i.e. cells, that cover the space of the lanes in a continuous way. An LGM has two parameters to be set: a cross-track cell width and an along-track cell length.

Fig. 4 shows an LGM representation of a merging intersection situation alongside a classical Cartesian Occupancy Grid (OG). The cells of the LGM are only located in areas of interest of the ego vehicle. Compared to an OG, an LGM is more compact, scalable and easier to manipulate, since information is encoded such that it fits the lane-level context that the ego vehicle encounters.

As shown in Fig. 4, the same area can be characterized differently by cells at junctions because of overlapping navigation corridors. This highlights that the cells are contextualized by the lanes they belong to.

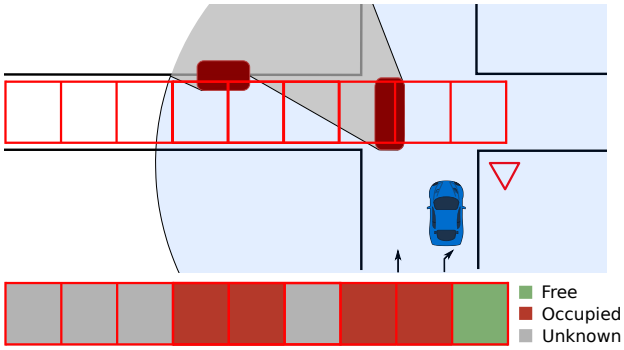

Fig. 5: Characterization process with polygons supplied by a perception module: free in blue, occupied in red and unknown in gray. The skeleton of the LGM is shown above, and the final characterization below.

In the rest of this paper, we use only a simplified representation of the LGM, where the discretization is applied only in the along-track direction. This simplification means that each cell encompasses the entire track width in the lateral direction. The LGM is therefore defined by a set of cells $LGM = \{c_i | \forall i \in [0; N]\}$ where each cell c_i is represented as a bounded interval of curvilinear abscissa $[\underline{c}_i; \overline{c}_i]$ along the lanes.

B. Occupancy characterization

Once the skeleton of an LGM has been constructed using the IG, the objective is to establish the spatial occupancy of each cell on the basis of information provided by a perception module, using a 3D Lidar for instance [30].

Fig. 5 is an illustration of the characterization process using an LGM. In this work, we assume that a perception module provides the free space characterized as a polygon [20] and a list of detected road users also represented by polygons. In Fig. 5 the perception module detects two road users, depicted by the two red objects. It also computes the free space within the range of the sensor. A cell in the LGM is considered to be occupied if it intersects with an object, and it is considered free if it is fully included within the free space. Otherwise the cell is designated as *unknown*. [7].

C. LGM integrity

With an LGM representation, integrity is the ability to supply non-misleading information to decision-making systems. For example, characterizing a driving space as free when it is actually occupied may lead to a collision.

The grid's sampling step parameter determines the level of detail to be used for the lane. The larger the cells, the coarser the information, calling for more cautious decision-making. Conversely, oversampling can lead to a loss of integrity resulting from the imperfect input coming from the perception system, which may give rise to decisions that are hazardous.

1) Experimental methodology for evaluating LGM integrity: To evaluate the integrity level of a given LGM we previously developed an experimental methodology in [31]. The integrity metric on which this rests is presented below. Our methodology involves carrying out experiments with several vehicles equipped with a localization ground truth. Fig. 6 shows three vehicles that were used to carry out the experiments. The blue car is the ego vehicle whose LGM is being evaluated. This vehicle is equipped with a Lidar sensor (a Velodyne VLP-32C) with a 360° field of view, a theoretical range of 100 meters, and running at 10 Hz. An HD map of the city of Compiègne was used as prior information to build the IG and the LGM. During the evaluation experiments we ensured that only the gray truck and white car shown in Fig. 6 were in the lanes of interest of the blue vehicle. This allowed us to acquire datasets without other road users for which we did not have a ground truth.

Fig. 6: Experimental vehicles (white car and gray truck behind the blue car) in Compiègne (France).

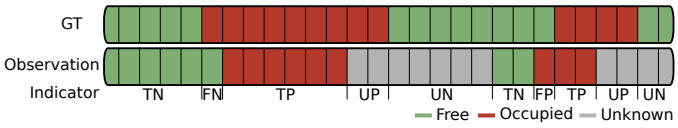

Fig. 7: Ground truth (above) and observed (below) LGMs.

2) LGM ground truth generation: Post-processed GNSS PPK corrections were used to have a centimeter-level localization of each vehicle at a rate of 50 Hz. To get an LGM ground truth at each time instant, the characterization process was performed using the ground truth position of the three vehicles recorded in the dataset. In other words, this was done without using the perception system. Given the accurate pose of the vehicles on the road and their dimensions, their occupancy was approximated by 2D bounding rectangles. Any cell overlapped by these rectangles was considered occupied, and the remaining cells were considered free. The cells of the ground truth LGM are all therefore either Free (F) or Occupied (O).

TABLE I: Construction table for the indicators: True/False (T/F), Positive/Negative (P/N), and Unknown (U). (red: misleading and hazardous, green: non-misleading, gray: undetermined, yellow: misleading but non-hazardous)

	Observation		
Ground Truth	Occupied	Free	Unknown
Occupied	TP	FN	UP
Free	FP	TN	UN

TABLE II: Aggregation rule for two cells. $Cell_{res}$ corresponds to the result of the fusion of the cells $Cell_i$ and $Cell_{i+1}$.

	$Cell_{i+1}$		
$Cell_i$	O	F	U
O	O	O	O
F	O	F	U
U	O	U	U

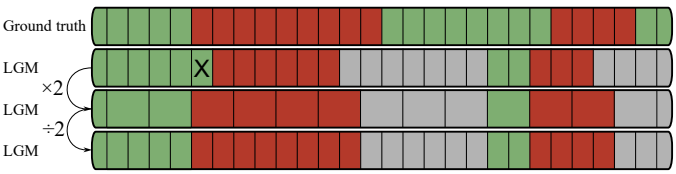

Fig. 8: The cells are aggregated two by two then separated back for evaluation. The false negative cell marked with a cross disappears after cells aggregation.

3) Integrity metric: Combining the different configurations, for each cell of the LGM there are six possible indicators obtained from the combination of the two characterizations as defined in Table I. The correspondence is shown in Fig. 7.

Two indicators are of interest. FP corresponds to free cells misclassified as occupied. This is an overcautious indicator that does not induce a safety problem. FN is the most important indicator in terms of integrity, as it corresponds to occupied cells misclassified as free. It is a misleading indicator that should occur as little as possible. If the space around the vehicle is considered free whereas in reality it is occupied, this may lead to a hazardous decision-making. The additional indicators UP and UN are not considered misleading, since here the cell state is unknown and consequently does not provide any information (free or occupied) that potentially may be misleading.

To evaluate the integrity, we therefore compute the frequency of occurrence of the FN indicator. This measure considers only cells that have been characterized as free or occupied, i.e. missing information is excluded. The False Negative Rate (FNR), also called the "miss rate", is the frequency of FN over all occupied cells, and is given by:

$$FNR = \frac{FN}{FN+TP} \tag{1}$$

In the remainder of the paper we seek to build a mechanism to maintain the FNR below a given threshold termed the Target Integrity Risk (TIR), which is set beforehand in line with a specific application's safety requirement.

4) Sampling strategy: We show in this study that the sampling step is able to control the integrity level of the information provided by an LGM, according to a given operational design domain. One of LGM's major contributions is therefore its ability to manage the integrity of the information, thanks to its capacity to control the FNR via the sampling step.

In order to tune the sampling step, we propose a methodology as shown in Fig. 8. Typically the step is chosen to be the one of the ground truth. To increase the sampling step, the cells can be aggregated. For instance, to have a sampling step twice as large, the cells are combined two by two using the aggregation rule presented in Table II. Then, to perform the comparison with the ground truth, the aggregated cells are separated back into the initial sampling step, as shown by the last row in Fig. 8. We can see that the case of FN has been replaced by a case of TP, which is no longer misleading.

It should be noted that the aggregation rule can also be used in real time to obtain an LGM with a desired sampling step, depending on an application's specific needs with respect to situation understanding.

5) Results: Here we report experimental results showing that it is possible to set a sampling step for a given TIR. A dataset containing sensor data was recorded using three vehicles in real road conditions. The ego vehicle was following the two others along a 2.1km trajectory. The polygons of the perceived vehicles were used to compute the LGM results [32]. A simple geometric ground fitting based on the Principal Component Analysis algorithm and a clustering algorithm was used on point-cloud data to extract object clusters surrounding the ego vehicle [33]. The geometric layer of the HD map was used to retain only clusters that were completely or partially on the road. At each Lidar scan, a free space polygon was generated over a radial grid using the shortest distance between the points of the clusters. The clusters were then tracked in order to compute estimates of their heading and speed, in order to be able to represent road users as objects in the form of polygons. To simulate different levels of imprecision in the detection of the road users, we added random Gaussian noise with different standard deviations to the detected polygons.

Fig. 9 shows that FNR falls as the sampling step increases. As the number of cells classified as occupied grows, these occupied cells cover a larger area, encompassing nearby cells that were incorrectly classified as free because of the localization error. Conversely, oversampling the LGM produces more misleading information, since FNR increases as the sampling step gets closer to zero.

As the standard deviation of the noise increases, FNR decreases, but at a higher level. This shows that it is possible to control FNR under a given integrity risk by increasing the sampling step. For example, if a maximum integrity risk of $0.3\,\%$, i.e. typically the risk associated with a 3σ Gaussian confidence interval, is specified for FNR, the integrity requirement can be met by setting the sampling step to the value shown by the red dots in Fig. 9.a. To compute these red dots, the different curves were interpolated in a logarithmic scale (dashed curves) and intersected with the required TIR. For a localization error with a $0.5\,\mathrm{m}$ standard deviation, a sampling step of $3.0\,\mathrm{m}$ is needed, while for a standard deviation smaller than 0.2, a sampling step lower than $1\,\mathrm{m}$ is enough. In other words, this graph shows that if the system is not able to properly model the localization uncertainty, a correctly chosen sampling stem can ensure the level of integrity as defined by the functional domain. For a given TIR, the greater the uncertainty, the larger the sampling step.

Note that even without adding noise (red curve), the minimal sampling step needs to be increased to at least 20 cm, in order to cover various unmodeled residual errors from the perception and the localization ground truth.

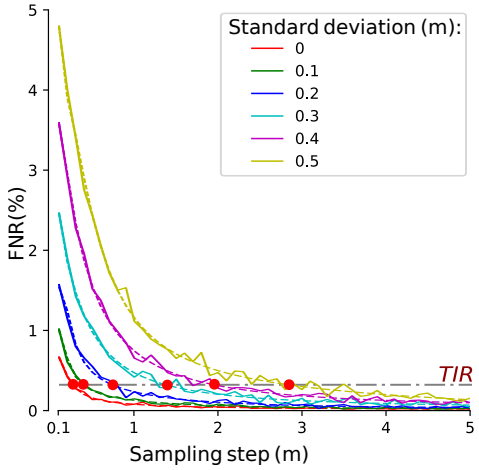

Fig. 9: FNR of the LGM with respect to the spatial sampling with different levels of noise on the positions of the detected vehicles.

IV. LGM PREDICTION

Once the autonomous vehicle has built an LGM at a given time t_0 using its own sensors, the next step is to predict the evolution of this representation over time. We use the notation $LGM(t|t_0)$ for any time t in a time horizon $[t_0; t_0 + \Delta t]$. Prediction allows the decision-making module to plan actions over a given time horizon.

In order to avoid dangerous decisions, prediction needs to remain consistent without introducing misleading information. This section shows how the same spatial sampling step strategy can be extended such that a given required integrity level can be reached, regardless of the accuracy of a given object-level prediction module.

Reachable sets are easy to represent in a predicted LGM, since they can be seen as a list of polygons. As a consequence, the same characterization process can be applied. The higher the sampling rate, the finer the representation. Reachable sets can therefore be seen as a finer representation of an LGM. Where the cross-track and along-track sampling steps of an LGM tend to zero, this representation tends to be continuous and thus leads to the classical the reachable sets formalism. As sampling steps increase in size, outer approximations are made and the discrete LGM representation encompasses the continuous case.

A. Prediction characterization

In the static LGM presented in the previous section, the characterization space was separated into three classes, namely: *Free*, *Occupied* and *Unknown*. In the prediction space, on the other hand, the two relevant classes are *Reachable* and *Non-Reachable*. A cell characterized as *Reachable* at a given time t means that a road user could potentially reach the cell at that time t. In particular, a cell with an *Unknown* state will be considered as *Reachable* because a potential hidden road user could be located in the cell. Conversely, a cell characterized as *Non-Reachable* means that no road user, visible or hidden, can reach it, which is equivalent to the *Free* state. In the rest of the paper, *Free* and *Non-Reachable* are considered equivalent.

B. Reachability for prediction

The prediction stage first initializes every cell in the predicted $LGM(t|t_0)$ as free (F). The reachability of road users and hidden space is then addressed.

1) Road users: In this paper we are not interested in building a novel object predictor, but we take as input a given module and integrate it into the LGM prediction framework. Therefore, for a given road user, we assume that an object predictor first computes the bounds along the center line of the road lane as an along-track curvilinear abscissa interval

$$\mathbf{s}(t) = [\underline{s}(t); \overline{s}(t)]\,, \tag{2}$$

which can be seen as a simplified one-dimensional reachable set.

The lateral prediction of a road user is handled along its taken path. It is assumed that a road user prediction may extend along several paths, as long as these paths belong to the LGM. The ability of a vehicle to drive on a path outside the LGM has no relevance for the ego vehicle, since being outside the LGM implies that there is no further interaction with this vehicle.

2) Hidden space: The same principles are applied in handling the hidden space. The hidden space may contain road users. If there are hidden vehicles, their lengths are unknown. Therefore, in the worst case, every cell may contain a potential road user whose speed is unknown. Equivalently, a single virtual road user can be considered, aggregating several contiguous hidden cells such that the interval $\mathbf{s}(t_0)$ corresponds to the bounds of a virtual road user. The bounds are predicted as the worst case scenarios, corresponding to a constant velocity equal to zero or to the maximum allowed velocity $v_{\lim}$:

$$\begin{cases} \underline{s}(t_0 + \Delta t) &= \underline{s}(t_0) \\ \overline{s}(t_0 + \Delta t) &= \overline{s}(t_0) + v_{\lim} \times \Delta t \end{cases} \tag{3}$$

C. LGM update

Once bounds of road users and hidden cells have been computed, the predicted $LGM(t|t_0)$ is updated with this new information. For this purpose, we define the reachability function as follows.

Definition 4.1 Reachability function

The reachability function R defines the cells c of the predicted $LGM(t|t_0)$ that are reachable. For each predicted entity (real or virtual road user) that at time t is contained within an interval $\mathbf{s}(t) = [\underline{s}(t); \overline{s}(t)]$, the set of reachable cells $R(\mathbf{s}(t))$ in the predicted $LGM(t|t_0)$ is defined as all the cells c that intersect $\mathbf{s}(t)$.

$$R(\mathbf{s}(t)) = \{c \in LGM(t|t_0) | c \cap \mathbf{s}(t) \neq \emptyset\} \tag{4}$$

All the reachable cells are updated as such.

Fig. 10 shows the prediction stages with the LGM update and the reachability function applied to two road users for a time horizon Δt. Fig. 10a shows an $LGM(t_0)$ that has cells with free, occupied and unknown states at time t_0. Two vehicles V_1 and $V_{virtual}$ are considered (the ego vehicle is not represented). In Fig. 10b, the predicted bounds of the road users are represented with dotted lines. The cells that

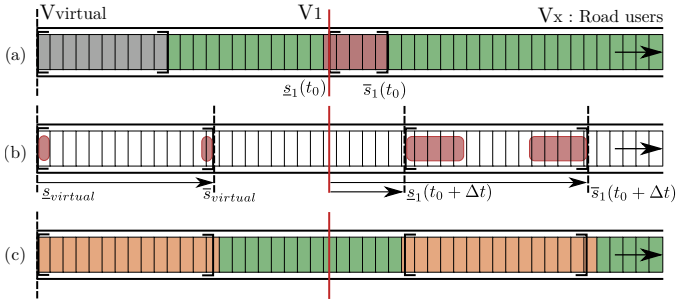

Fig. 10: Processes for building a predicted $LGM(t_0 + \Delta t|t)$ with a virtual and a real road user. (a) $LGM(t_0)$ with free (green), hidden (gray) and occupied (red) cells. The rear boundary of vehicle V_1 is represented by a dotted line. (b) Upper and lower bounds of the predicted road users. (c) The predicted LGM is updated in orange with possibly occupied states.

TABLE III: Correspondence between the predicted states of $LGM(t|t_0)$ with the true states of $LGM(t)$.

True $LGM(t)$	Predicted $LGM(t\|t_0)$	
	Reachable	Non-reachable
Occupied	Non-Misleading (1)	Hazardous (2)
Free	Non-Hazardous (3)	Non-Misleading (4)

encompass the prediction bounds of each vehicle are retrieved. In Fig. 10c, the $LGM(t|t_0)$ is updated with reachable cells (orange). The prediction of hidden cells is similar to the prediction of objects, with the assumption that the length of a virtual road user corresponds to the size of the aggregated hidden cells.

D. Integrity: FNR evaluation

The integrity of the prediction is now addressed. The purpose is to show how the integrity of information can be controlled regardless of the performance of the prediction model. Let consider a road user prediction on a single lane. Table III shows the types misleading information that can be produced by the predicted LGM, analogously to the concept of integrity in the static LGM. Here, it is hazardous to define as non-reachable an area that in reality is occupied, since this may induce wrong decision-making.

To illustrate the management of integrity management we built a family of custom naive object predictors with constant unknown acceleration, providing the following curvilinear abscissa bounds:

$$\begin{cases} \underline{s}(t_0 + \Delta t) = \underline{s}(t_0) + \underline{v}(t_0) \times \Delta t + \frac{1}{2}\underline{a}(t_0) \times \Delta t^2 \\ \overline{s}(t_0 + \Delta t) = \overline{s}(t_0) + \overline{v}(t_0) \times \Delta t + \frac{1}{2}\overline{a}(t_0) \times \Delta t^2 \end{cases} \quad (5)$$

where s is the curvilinear abscissa, v the velocity and a the acceleration under the hypothesis that the acceleration remains constant in the time interval $[t_0, t_0 + \Delta t]$ and that the velocity is positive and bounded by $v_{\lim}$, the maximum allowed velocity. Note that this predictor could be replaced by any other predictor from the literature.

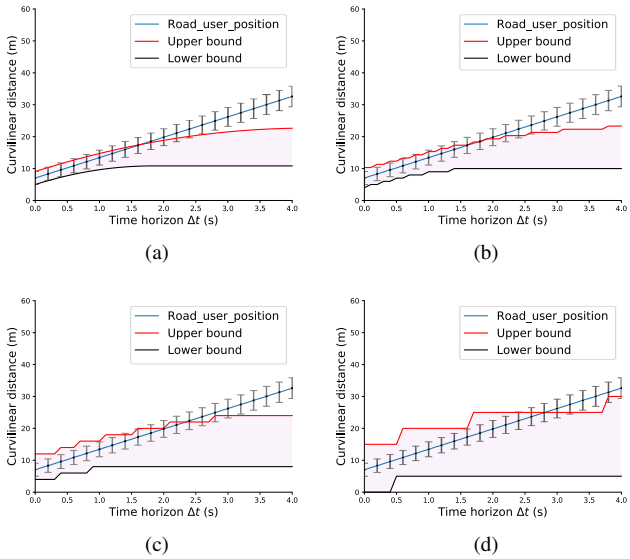

Fig. 11: The road user position (blue) is modeled with an upper and lower bound (rear and front). The reachable distance is filled by the purple area. The lower bound of the CD model corresponds to the black curve and the upper bound to the red curve. (a) reachable area with a sampling step that tends to $0.0\,\mathrm{m}$ (b) reachable area with a sampling step of $1.0\,\mathrm{m}$, (c) $2.0\,\mathrm{m}$, (d) $5.0\,\mathrm{m}$.

1) Simulated results: As an initial step, to make it easier to understand the experimental results, we did some simulations. Given the LGM of a straight lane, we consider a single road user traveling in accordance with a Constant Velocity (CV) model, i.e. Eq. 5 is used with $a = 0\,\mathrm{m.s^{-2}}$. Then, to highlight the integrity management mechanism, we deliberately choose, for the road user prediction, an inaccurate Constant Deceleration model (CD), with $a(t) \in [-1.5; -3.5]\mathrm{m.s^{-2}}$. At a given time t_0, the predicted $LGM(t|t_0)$ is generated over $4.0\,\mathrm{s}$. This simulation allows us to compare directly the true evolution of a road user (which is known) with a given evolution model. The purpose is to show how, even with an approximate evolution model, the sampling step parameter can ensure the integrity of the prediction information.

Fig. 11 shows simulated results for the vehicle driving on a straight lane at constant speed (blue line) with the CD model. The figure shows to what extent predicted bounds encompass, or fail to encompass, the whole body of the vehicle at each prediction time. The vehicle's body is modeled by its position (the center) with an upper and lower bound (rear and front). The predicted bounds are represented in a continuous space dimension, which is equivalent to setting a sampling step close to zero. From Fig. 11a it will be remarked that the CD model does not encompass the true position as the time horizon increases. The goal is now to show how misleading information is managed.

Fig. 11d shows the smallest sampling step that enables the predicted reachable bounds to encompass the vehicle position for at least $2.0\,\mathrm{s}$ of prediction. Since the CD model does not bound the road user position, a sampling step of $5.0\,\mathrm{m}$ is chosen in order to overestimate the reachable area. From Fig. 11b it can be seen that a sampling step of $1.0\,\mathrm{m}$ fails to

encompass the true position over the interval. As the sampling step increases (see Fig. 11c), the encompassing of the road user position improves. In stark contrast to Fig. 11a, and according to the target integrity risk, integrity is maintained for $2.0\,\mathrm{s}$ of prediction by using a larger sampling step. In a similar way, the sampling step may be increased in order to maintain integrity over a larger Δt horizon.

If the prediction model is reliable for a short prediction time and then drifts, a sampling step can be set in accordance with the relevant time horizon. As a consequence, even with an extreme case such as the CD model, a very large sampling step means that the whole lane can be defined as reachable. Here, although the information has a high degree of integrity, the decision-making process will clearly be impacted towards considerable caution, since there are no longer any free cells.

As mentioned before, the goal here is to ensure that any misleading information is non-hazardous. For this purpose, the integrity of the system is defined as its ability to maintain statistically the FNR below a given threshold that is termed the Target Integrity Risk (TIR).

Fig. 12a shows the FNR for the same situation, but obtained using a range of different sampling steps. Because the CD model is an inaccurate model here, the FNR grows rapidly as the prediction time horizon increases. It can also be observed that for any given time horizon, increasing the sampling step reduces the FNR. The kinks in the curves are a side effect of the sampling step. This is because the cells defined as reachable depend on t_0. At this time, if the road user is close to the start or to the end of a cell, there will be an impact on the update function.

The true statistical FNR is obtained by averaging more than one thousand simulations varying the initial time t_0. It can be seen from Fig. 12b that whatever the given time horizon, the FNR decreases by as the the sampling step increases. Given a fixed TIR, this figure highlights the integrity property of the sampling step, which is similar to the integrity of a static LGM. The further away the predicted time, the higher the sampling step that is required in order to remain below the TIR.

2) Experimental results: Three sequences were recorded in a dataset for a situation where the ego vehicle was observing another experimental vehicle entering a roundabout on its left side. Fig. 13 shows the experimental results that are representative of Fig. 12a with a CD model. The actual evolution model of the human road user is unknown, and the curves suggest that the CD model is likely to be inaccurate.

In Fig. 13a, the evolution of the FNR with the CD model is shown for different sampling steps from 0.2 to 5 m. For any required prediction time horizon and TIR, it is possible to maintain the FNR below the TIR by increasing the sampling step. When the prediction time horizon increases, the bounds computed by the CD model are further away from the true road user position, thus requiring a much larger sampling step in order for the correct cell to continue to capture the road user. In contrast, where the evolution model is closer to the true evolution, e.g with a CV model, the bounds computed by the model will likely contain the true road user position (see Fig. 13b). The LGM can therefore be computed with a much smaller sampling step. We recall that prediction model

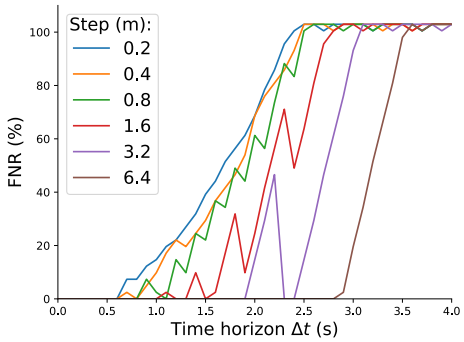

(a)

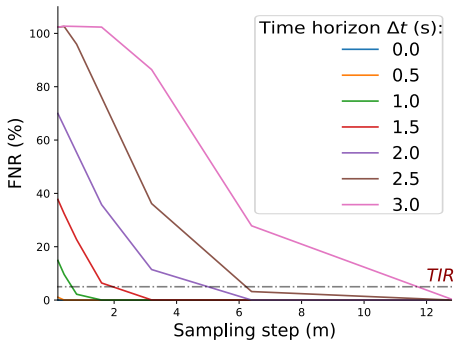

(b)

Fig. 12: Evolution of the FNR w.r.t. the time horizon for different sampling step using simulated data (CD model). (a) Single simulation. (b) Average over more than one thousand simulations. The further away from the origin, the more the curve corresponds to a distant predicted time horizon.

performance is not being evaluated here. If the prediction model is accurate enough to capture the road user position within the prediction bounds, then the requirement in terms of the sampling step will not be stringent. Conversely, if the prediction model is far removed from reality, the sampling step will act as a parameter for managing the integrity of the whole system.

However, increasing the sampling step can reduce the non-reachable space in the LGM. This results in an overestimation of the reachable space that can impact the decision-making towards an excess of caution. The consequence is a loss of functional availability for the autonomous navigation of a vehicle, which may, for example, remain stuck for a long time at an intersection when traffic is heavy.

V. Enhanced Space Characterization

This section shows how prediction may be improved by taking interactions into account. In order to strengthen decision-making, including under occlusion, the available and missing information in areas of interest needs to be quantified. With the aim of improving situation understanding in unknown areas, such as areas hidden by other road users, we developed a characterization process that applies reasoning on the basis of prior map information. Below we explain the concept of neutralization in relation to these unknown areas.

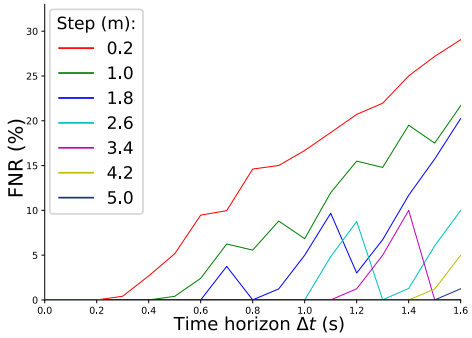

(a)

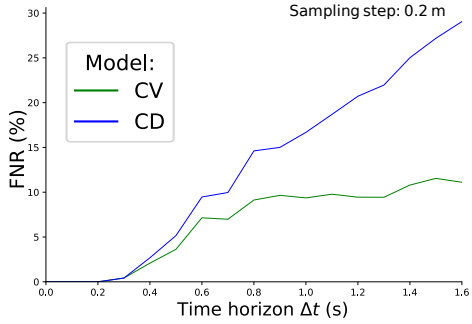

(b)

Fig. 13: (a) Evolution of the FNR of prediction with experimental results obtained with the CD model. Each curve displays the evolution for a given sampling step. (b) Evolution of the FNR of prediction for the CV and CD model with a sampling step of $0.2\,\mathrm{m}$.

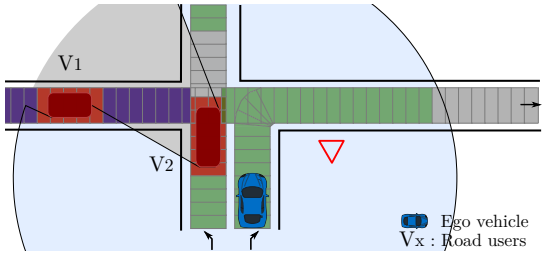

Fig. 14: LGM with a characterization of the neutralized cells on a T-intersection: Free (green), Occupied (red), Unknown (gray), Neutralized (purple).

A. Enhanced characterization process: the neutralized frame

An important aspect of the interaction between road users is that they impose physical constraints on each other. Once a road user occupies a given space on the road, no other road user can cross this space without causing an accident.

Fig. 14 presents a situation where a neutralized area is caused by a dynamic object. The vehicle V_2 is protecting the ego vehicle from road users coming from the left, e.g. V_1. It is physically engaged and thus induces a neutralized area as shown in purple. It must be noted that the neutralized area may reach outside of the field of view of the ego vehicle. As it is neutralized by a perceived road user, the ego vehicle has the possibility to take a decision under occlusion.

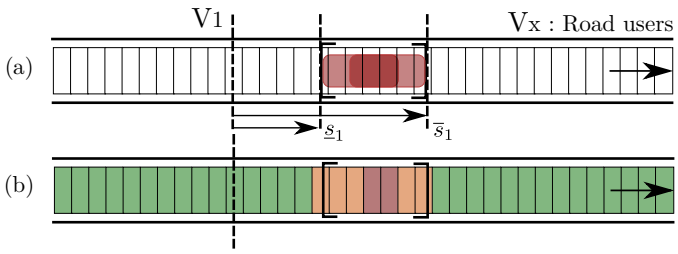

Fig. 15: Illustration of prediction stages with occupancy prediction at time horizon Δt. (a) Model-based object prediction with upper and lower bounds and with an overlap. The footprint of the vehicle is shown at the two ends of the reachable set. (b) Final predicted $LGM(t_0 + \Delta t|t_0)$ with an additional occupied state in red.

The neutralized property is only relevant within the unknown category. In Fig. 14, the neutralized property can be ignored where a perceived road user is present as the occupied knowledge is more informative.

B. Prediction with neutralization

When a neutralized area has been characterized in the current LGM, its status can also be predicted.

Suppose that there is an initial neutralized situation at time t_0. As a consequence, during the prediction, a key point is to estimate how long the situation will remain with a neutralized lane, since this allows the ego vehicle to navigate while remaining protected. The duration of this neutralization is called Neutralized Time Interval (NTI).

In order to determine if cells are neutralized at a time $t = t_0 + \Delta t$, we need to look for occupied cells that may cause the lane to be neutralized. Only a cell that is fully occupied can generate a neutralized area. It is therefore crucial to characterize the cells that are truly occupied during the reachability analysis.

1) Occupancy: Reachable cells can be occupied, with the U state, or truly occupied, with a state O. A cell is considered occupied if it is completely overlapped by the footprint of a road user placed at the bounds of $\mathbf{s}(t)$ (see Fig. 15). As a consequence, a partially occupied cell is considered only as reachable, since it is not actually fully occupied. Road user lengths L are supplied by the object tracker.

The footprint occupancy is defined as follows.

Definition 4.2 Footprint occupancy

For a given road user in the interval $\mathbf{s}(t)$, its footprint occupancy $\mathbf{s}_L(t)$ is defined by:

$$\mathbf{s}_L(t) = \begin{cases} [\overline{s}(t) - L; \underline{s}(t) + L] & \text{if } \underline{s}(t) + L > \overline{s}(t) - L \\ \emptyset & \text{otherwise} \end{cases} \tag{6}$$

The predicted $LGM(t|t_0)$ is updated with this information. An occupation function is defined as follows.

Definition 4.3 Occupation function

The occupation function O of road users defines cells of the predicted LGM with an occupied state O. The set of predicted occupied cells $O(\mathbf{s}_L(t))$ is defined as all the

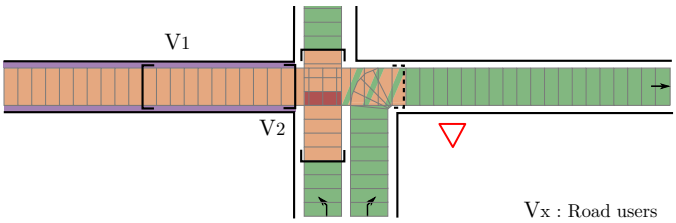

Fig. 16: Backward propagation of the neutralized constraint on a predicted LGM at time $t_0 + \Delta t$. The purple area remains neutralized since V_2 is guaranteed to occupy at least one cell (in red) of the crossing area during the entire prediction horizon. The hatched area is therefore removed, since these cells are no longer reachable.

cells c in the predicted $LGM(t|t_0)$ that are included in $\mathbf{s}_L(t)$:

$$O(\mathbf{s}_L(t)) = \{c \in LGM(t|t_0) | c \subseteq \mathbf{s}_L(t)\} \quad (7)$$

All the predicted occupied cells are updated with the label *Occupied*.

Fig. 15 illustrates a predicted LGM update using the occupation function, given a road user V_1 and a time horizon Δt. The footprint of V_1 is placed at each end of the predicted bounds. The cells that are within the overlapping bounds are retrieved. Note that if the predicted interval $\mathbf{s}(t)$ is twice as long as the road user length L, then there is no occupancy. It will be remarked that hidden cells cannot generate occupancy, but only reachability, since prediction is done only with respect to virtual vehicles. There is no guarantee that these virtual vehicles correspond to real physical road users.

2) Neutralization: We now focus on the prediction of an LGM with a lane characterized initially as neutralized.

In this problem, applying a constraint on a vehicle prediction is dependent on the prediction of another road user. Prediction of cells located in a neutralized area is constrained if and only if this area remains neutralized. An area can remain neutralized only if there has been a prediction of another road user that has given rise to this situation. At first glance it would appear complicated to make predictions of road users that are dependent on others, since the number of predictions can increase dramatically in some complex driving situations. That is why all the road users are first predicted independently w.r.t. each other without any constraint. The physical interaction induced by neutralization is then back-propagated onto the reachable cells of the road users and the hidden cells located in the neutralized areas. This prevents prediction of some cells from reaching non-reachable areas.

For a predicted $LGM(t|t_0)$, there are two possible scenarios:

a) The neutralized area remains neutralized in the predicted LGM at time $t_0 + \Delta t$ (see Fig. 16). As a consequence, a constraint is applied on reachable cells which were generated by road users or potential road users in the neutralized area. This backward constraint propagation is defined as follows.

Definition 4.4 Backward constraint propagation

Let the set $\{\mathbf{s}_1(t_0), \mathbf{s}_2(t_0), \ldots\}$ be the set of entities (real or virtual road users) that are in the neutralized area $\mathcal{N}$ at time t_0. At a given time $t = t_0 + \Delta t$, let $\mathcal{O}(t) = R(\{\mathbf{s}_1(t), \mathbf{s}_2(t), \ldots\})$ be the reachable cells of all these entities. Assuming that $\mathcal{N}$ is still neutralized in the predicted $LGM(t|t_0)$, all the cells in $\mathcal{O}(t)$ that are outside the neutralized area $\mathcal{N}$ defined as

$$\mathcal{C} = \mathcal{O}(t) \backslash \mathcal{N} \quad (8)$$

are actually not reachable by the entities in $\mathcal{N}$.

The backward constraint propagation consists in canceling all the updates that have been applied to the cells in $\mathcal{C}$ by any entity $\mathbf{s}_i$. As a result, in Fig. 16, the backward constraint propagation is applied on the cells that are located outside the neutralized area. The difference can be seen where cells are set to free instead of unknown.

b) The neutralized area is no longer neutralized in the predicted LGM at time $t_0 + \Delta t$. No backward propagation is applied.

TABLE IV: Correspondence between the predicted states of $LGM(t|t_0)$ and the true states of $LGM(t)$.

True $LGM(t)$	Predicted $LGM(t\|t_0)$		
	Occupied	Reach.	Non-reachable
Occupied	Non-Misleading (1)		Hazardous (2)
Free	Hazardous (neutr.)	Non-Hazardous (3)	Non-Misleading (4)

3) Integrity: This section is concerned with managing the integrity of the information provided by the predicted LGM, taking into account the neutralized situation. In comparison with the integrity study presented above (see Table III), there is a new hazardous situation (see Table IV). Up to now, a false positive, that is predicting a free cell as occupied or reachable, was considered non-hazardous, given that any resulting inappropriate behaviour is likely to be excessively cautious rather than insufficiently so. With the introduction of the concept of neutralization, a cell that is wrongly predicted as occupied may lead to false neutralization constraints, which can imply hazardous decisions.

As a consequence, the FNR metric that we have used so far is no longer sufficient to guarantee system integrity. An additional metric is needed to address this new hazardous situation. For this purpose we compute the duration of the neutralization constraints, termed NTI (Neutralized Time Interval). This performance metric corresponds to the last predicted time $t_{NTI} = t_0 + NTI$ for which a neutralized area remains. Computing the NTI when a neutralized area occurs means finding the earliest time for which there is no longer any fully occupied cell in the crossing area. The implementation consists in predicting the LGM over a time horizon with a given sampling time δt and simply identifying the first time when the neutralization ends. It corresponds to a lower bound approximation of the actual NTI.

The goal is to compute a value that is as close as possible to, but does not exceed, the real NTI. Overestimating the NTI may lead to hazardous situations, e.g. the ego vehicle estimates that it has enough time to cross while in reality it does not. Conversely, underestimating the NTI leads to

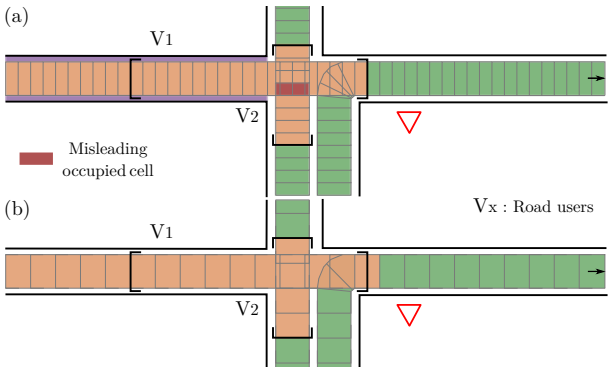

Fig. 17: Two $LGM(t|t_0)$ computed with different sampling steps. As the sampling step increases, the misleading information due to a prediction error disappears. The situation is therefore no longer considered neutralized.

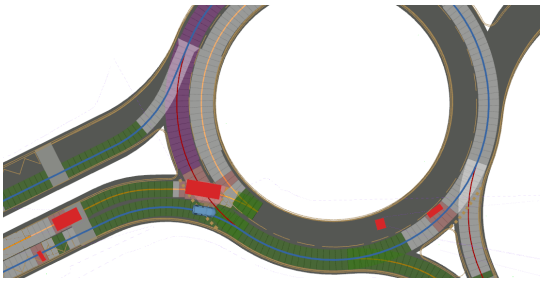

Fig. 18: LGM representation at a roundabout in a real-time experiment in Compiègne. The ego vehicle (blue) enters the roundabout with a vehicle on its left side (red). This vehicle located on the secondary order lane causes an occlusion. As it is already engaged, the primary order lane is neutralized (purple). Free cells are shown in green, and occupied cells in red. Other cells in gray are partially or completely hidden.

overcautious decisions: the integrity of navigation information is guaranteed, but the availability of the navigation function is reduced.

The quality of the estimated NTI depends on the prediction of the road users. For example, in Fig. 17, a mistakenly neutralized area is assumed with a sampling step of $1\,\mathrm{m}$. The upper bound of the road user V_2 has been underestimated. In Fig. 17a, at some time t in the future, the LGM predicts that a cell will be fully occupied when it is not. This generates a neutralized area that may lead the ego vehicle to decide to cross. This situation leads to an overestimation of the NTI.

We have already demonstrated that enlarging the sampling step provides a means of handling system integrity in terms of FNR. Fortunately, the same process can also be used for controlling integrity in terms of NTI. As the sampling step increases, for a given prediction time, the state of an occupied cell changes to unknown, meaning that potentially a wrongly neutralized area may disappear, once there are no remaining occupied cells (see Fig. 17b).

C. Real experimental results

1) Implementation: The LGM generation and its characterization process were implemented on a Renault ZOE experimental vehicle belonging to the Heudiasyc Laboratory using ROS middleware. The computer used had an Intel i7 (7th) processor and $16\,\mathrm{Go}$ of RAM. For the computation of the IG, a distance of interest of $100\,\mathrm{m}$ was chosen, and for the LGM an arbitrary cell discretization step of $1\,\mathrm{m}$ was set in order to achieve real-time performance. The LGM was generated at a frequency of $10\,\mathrm{Hz}$ and the IG at $0.25\,\mathrm{Hz}$.

2) Case study: In Fig. 18, a neutralized area is shown in a roundabout entrance situation. The ego vehicle intends to enter the roundabout by merging with the outer lane. Since the vehicle on the left belongs to the lane to the left of the ego vehicle and is crossing the merging lane, the area behind that vehicle is therefore characterized as neutralized. This is the situation addressed in our computation of $LGM(t_0)$.

3) Results: To compute the bounds for a given prediction Δt horizon, Eq. 5 is used with different intervals for the acceleration. The following three models, labeled according to their upper bound on the acceleration, are considered in order to evaluate their impact on the results:

1) Constant acceleration (CA): $a(t) \in [-3.5; 4.0]\ \mathrm{m.s^{-2}}$
2) Constant velocity (CV): $a(t) \in [-3.5; 0.0]\ \mathrm{m.s^{-2}}$
3) Constant deceleration (CD): $a(t) \in [-3.5; -1.5]\ \mathrm{m.s^{-2}}$

For each model, the velocity is also constrained within the interval $[0; v_{\mathrm{lim}}]$, i.e. the vehicle cannot travel backwards or faster than the speed limit (where $v_{lim} = 50.0\,\mathrm{km.h^{-1}}$ in the roundabout). They all have the same lower acceleration bound. The model used for hidden cells is based on Eq. 3 where $v_{lim} = 50.0\,\mathrm{km.h^{-1}}$. We therefore have a constant velocity model.

In order to store the predicted LGM, each cell of the LGM has a vector of its predicted states. When a neutralized area is encountered, as described above, the prediction process is launched. Given a maximum prediction time horizon $\Delta t_{max} = 2\,\mathrm{s}$ and a time sampling step of $0.1\,\mathrm{s}$, each predicted $LGM(t|t_0)$ is computed based on the initial $LGM(t_0)$ and the neutralized constraint is applied depending on the situation. The neutralized constraint is back-propagated if and only if the neutralized area remains neutralized. This gives the predicted NTI. Once the constraint is no longer applicable, the predicted NTI is used for the reachability analysis of the neutralized cells. Cells outside the neutralized area start to be reached after the NTI has elapsed.

In order to show how integrity is handled through the prediction process, a number of different sampling steps were used for the predicted LGM.

The results that are presented in this section serve a twofold purpose. First, they demonstrate the advantage of the neutralized constraint. It is possible to make a prediction that remains consistent and that is able to improve the reachability analysis, and thus the decision-making process, throughout the NTI. Second, they show that an appropriate tuning of the sampling step parameter can prevent this prediction representation from generating misleading information.

The impact of the sampling step parameter on the predicted neutralized time interval is shown in Fig. 19. The different curves represent the evolution of the NTI using different prediction models for the road users: CD (blue), CV (green),

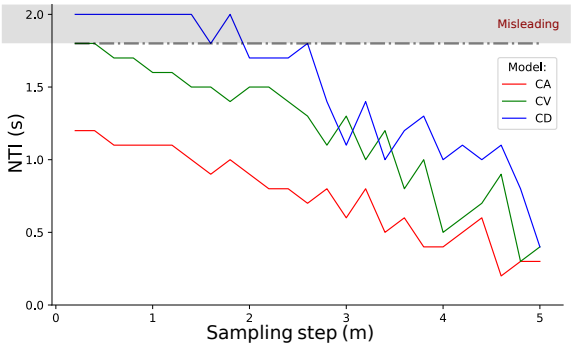

Fig. 19: Evolution of the predicted NTI obtained as a function of the sampling step. The three models CA, CV and CD are represented respectively by the red, green and blue curves. The NTI computed with the $LGM(t)$ is shown as the dotted line. Values above this line are considered misleading.

CA (red). With all three models it can be seen that that higher the sampling step, the lower the predicted NTI.

The NTI obtained with the $LGM(t)$ observed in replay is shown as a horizontal gray line. A misleading situation occurs where the estimated NTI is larger than the true NTI, as in the case of the CD model. By increasing the sampling step, the NTI is no longer misleading, even with an approximate model. The CV model is able to maximize the NTI, while the CA model is much more conservative but also more robust. With a more pessimistic model, it becomes harder to predict a long NTI, and the resulting situation understanding is therefore more conservative. Results show how the sampling step can maintain integrity by ensuring a lower estimation of the predicted neutralized time interval. The CD prediction model demonstrates the loss of integrity when a model does not bound the real behavior of road users. In order to fulfill the same requirement, the sampling step needs to be increased up to two meters at least. It will be remarked that the maximum NTI that can be obtained is bounded by the maximum predicted time horizon, $\Delta t = 2\,\mathrm{s}$ in this case.

VI. Conclusion

The Lane Grid Map is a lane-level representation that allows the driving situation of an autonomous vehicle to be modeled at an intermediate level by taking into account topological information from an HD map. Since this representation is used by a decision-making system, the integrity of the information that it contains needs to be controlled over a time horizon in order to avoid providing misleading information. We have shown how an LGM can make a prediction model reliable, even if it is inevitably an imperfect reflection of reality. This is achieved by setting an appropriate sampling step for the LGM, such as to maintain the integrity below a given Target Integrity Risk. The general principle is that the False Negative Rate can be reduced as needed by increasing the length of the sampling step. This strategy can lead to a loss of availability of the driving system as the vehicle becomes overcautious. For this reason, we have proposed an improvement that takes interactions into account interactions via the concept of neutralization, which can improve decision-making in some situations without compromising safety. Interactions are taken into account with the NTI metric, and we have shown that a similar sampling step tuning procedure is also able to guarantee the integrity of the prediction in these situations.

Once an object predictor has been set, along with the integrity requirement of the decision-making module in terms of prediction time horizon and TIR, a data collection step is required in order to tune the integrity performance and select the optimal sampling step satisfying the integrity requirement while maximizing the availability. Because this strategy is data driven, finding a robust optimal sampling step requires a large quantity of recorded driving recording data for all the target operational domain designs.

In this paper, we have considered a simplified LGM with a space discretization in the along-track direction and with a single sampling step. In future works, we will consider both the along- and cross-track directions, as well as sampling steps that are adaptive w.r.t. to the navigation task, in order to further increase the availability of the system.

Acknowledgments

This work has been carried out within SIVALab, a shared laboratory between Renault and Heudiasyc. Equipment from ROBOTEX (ANR-10-EQPX-44-01) were used for the experiments. The authors would like to thank Antoine Lima, Stefano Masi and Stéphane Bonnet for their support in the experiments.

References

[1] M. R. Endsley, "Toward a Theory of Situation Awareness in Dynamic Systems," *HUMAN FACTORS*, p. 33, 1995.

[2] E. Vendrell, M. Mellado, and A. Crespo, "Robot planning and replanning using decomposition, abstraction, deduction, and prediction," *Engineering Applications of Artificial Intelligence*, vol. 14, no. 4, pp. 505–518, Aug. 2001.

[3] I. Miller, B. Schimpf, M. Campbell, and J. Leyssens, "Tightly-coupled GPS / INS system design for autonomous urban navigation," in *2008 IEEE/ION Position, Location and Navigation Symposium*, pp. 1297–1310.

[4] J. A. Hage, P. Xu, P. Bonnifait, and J. Ibanez-Guzman, "Localization Integrity for Intelligent Vehicles Through Fault Detection and Position Error Characterization," *IEEE Transactions on Intelligent Transportation Systems*, pp. 1–13, 2020.

[5] N. Zhu, J. Marais, D. Betaille, and M. Berbineau, "GNSS Position Integrity in Urban Environments: A Review of Literature," *IEEE Transactions on Intelligent Transportation Systems*, vol. 19, no. 9, pp. 2762–2778, Sep. 2018.

[6] F. Li, P. Bonnifait, and J. Ibañez-Guzmán, "Map-aided dead-reckoning with lane-level maps and integrity monitoring," *IEEE Transactions on Intelligent Vehicles*, vol. 3, no. 1, pp. 81–91, 2018.

[7] C. Sanchez, Ph. Xu, A. Armand, and Ph. Bonnifait, "Lane level context and hidden space characterization for autonomous driving," in *IEEE Intelligent Vehicles Symposium (IV)*, Las Vegas, NV, USA, Oct. 2020, pp. 144–149.

[8] S. Shalev-Shwartz, S. Shammah, and A. Shashua, "On a Formal Model of Safe and Scalable Self-driving Cars," *arXiv:1708.06374 [cs, stat]*, Aug. 2017.

[9] O. S. Tas, F. Kuhnt, J. M. Zollner, and C. Stiller, "Functional system architectures towards fully automated driving," in *IEEE Intelligent Vehicles Symposium (IV)*, Gotenburg, Sweden, Jun. 2016, pp. 304–309.

[10] A. Furda and L. Vlacic, "Enabling Safe Autonomous Driving in Real-World City Traffic Using Multiple Criteria Decision Making," *IEEE Intelligent Transportation Systems Magazine*, vol. 3, no. 1, pp. 4–17, 2011.

[11] S. Ulbrich, A. Reschka, J. Rieken, S. Ernst, G. Bagschik, F. Dierkes, M. Nolte, and M. Maurer, "Towards a Functional System Architecture for Automated Vehicles," *arXiv:1703.08557 [cs]*, Mar. 2017.

[12] S. Ulbrich, T. Menzel, A. Reschka, F. Schuldt, and M. Maurer, "Defining and Substantiating the Terms Scene, Situation, and Scenario for Automated Driving," in *IEEE 18th International Conference on Intelligent Transportation Systems*, Sep. 2015, pp. 982–988.
[13] J. A. Michon, "A Critical View of Driver Behavior Models: What Do We Know, What Should We Do?" in *Human Behavior and Traffic Safety*, L. Evans and R. C. Schwing, Eds. Boston, MA: Springer US, 1985, pp. 485–524.
[14] S. Ulbrich, T. Nothdurft, M. Maurer, and P. Hecker, "Graph-based context representation, environment modeling and information aggregation for automated driving," in *IEEE Intelligent Vehicles Symposium (IV)*, Jun. 2014, pp. 541–547.
[15] N. F. Heide, A. Albrecht, T. Emter, and J. Petereit, "Performance Optimization of Autonomous Platforms in Unstructured Outdoor Environments Using a Novel Constrained Planning Approach," in *IEEE Intelligent Vehicles Symposium (IV)*, Paris, France, Jun. 2019, pp. 2359–2364.
[16] J. Moras, V. Cherfaoui, and P. Bonnifait, "Credibilist occupancy grids for vehicle perception in dynamic environments," in *IEEE International Conference on Robotics and Automation*, Shanghai, China, May 2011, pp. 84–89.
[17] A. Elfes, "Using occupancy grids for mobile robot perception and navigation," *Computer*, vol. 22, no. 6, pp. 46–57, Jun. 1989.
[18] T. P. Michalke, C. Glaser, L. Burkle, and F. Niewels, "The narrow road assistant - evolution towards highly automated driving in inner city," in *IEEE Intelligent Vehicles Symposium (IV)*, Gotenburg, Sweden, Jun. 2016, pp. 1192–1198.
[19] J. Laconte, E. Randriamiarintsoa, A. Kasmi, F. Pomerleau, R. Chapuis, C. Debain, and R. Aufrère, "Dynamic lambda-field: A counterpart of the bayesian occupancy grid for risk assessment in dynamic environments," in *2021 IEEE/RSJ International Conference on Intelligent Robots and Systems (IROS)*, 2021, pp. 4846–4853.
[20] M. Schreier, V. Willert, and J. Adamy, "Compact Representation of Dynamic Driving Environments for ADAS by Parametric Free Space and Dynamic Object Maps," *IEEE Transactions on Intelligent Transportation Systems*, vol. 17, no. 2, pp. 367–384, Feb. 2016.
[21] S. Lefèvre, D. Vasquez, and C. Laugier, "A survey on motion prediction and risk assessment for intelligent vehicles," *ROBOMECH Journal*, vol. 1, no. 1, p. 1, Jul. 2014.
[22] A. Rudenko, L. Palmieri, M. Herman, K. M. Kitani, D. M. Gavrila, and K. O. Arras, "Human motion trajectory prediction: A survey," *The International Journal of Robotics Research*, vol. 39, no. 8, pp. 895–935, Jul. 2020.
[23] M.-Y. Yu, R. Vasudevan, and M. Johnson-Roberson, "Occlusion-Aware Risk Assessment for Autonomous Driving in Urban Environments," *IEEE Robotics and Automation Letters*, vol. 4, no. 2, pp. 2235–2241, Apr. 2019.
[24] S. Hoermann, F. Kunz, D. Nuss, S. Renter, and K. Dietmayer, "Entering crossroads with blind corners. A safe strategy for autonomous vehicles," in *2017 IEEE Intelligent Vehicles Symposium (IV)*. Los Angeles, CA, USA: IEEE, Jun. 2017, pp. 727–732.
[25] P. F. Orzechowski, A. Meyer, and M. Lauer, "Tackling Occlusions & Limited Sensor Range with Set-based Safety Verification," *2018 21st International Conference on Intelligent Transportation Systems (ITSC)*, pp. 1729–1736, Nov. 2018.
[26] P. Narksri, E. Takeuchi, Y. Ninomiya, and K. Takeda, "Crossing Blind Intersections from a Full Stop Using Estimated Visibility of Approaching Vehicles," in *2019 IEEE Intelligent Transportation Systems Conference (ITSC)*. Auckland, New Zealand: IEEE, Oct. 2019, pp. 2427–2434.
[27] M. Koschi and M. Althoff, "SPOT: A tool for set-based prediction of traffic participants," in *IEEE Intelligent Vehicles Symposium (IV)*, Los Angeles, CA, USA, Jun. 2017, pp. 1686–1693.
[28] ——, "Interaction-aware occupancy prediction of road vehicles," in *IEEE 20th International Conference on Intelligent Transportation Systems (ITSC)*, Yokohama, Oct. 2017, pp. 1–8.
[29] S. Manzinger, C. Pek, and M. Althoff, "Using Reachable Sets for Trajectory Planning of Automated Vehicles," *IEEE Transactions on Intelligent Vehicles*, vol. 6, no. 2, pp. 232–248, Jun. 2021.
[30] Y. Li and J. Ibanez-Guzman, "Lidar for autonomous driving: The principles, challenges, and trends for automotive lidar and perception systems," *IEEE Signal Processing Magazine*, vol. 37, no. 4, pp. 50–61, 2020.
[31] C. Sanchez, Ph. Xu, A. Armand, and Ph. Bonnifait, "Spatial Sampling and Integrity in Lane Grid Maps," in *IEEE Intelligent Vehicles Symposium (IV)*, Nagoya, Japan, Jul. 2021, pp. 190–196.
[32] E. Bernardi, S. Masi, P. Xu, and P. Bonnifait, "High Integrity Lane-level Occupancy Estimation of Road Obstacles Through LiDAR and HD Map Data Fusion," in *IEEE Intelligent Vehicles Symposium (IV)*, Oct. 2020, pp. 1873–1878.
[33] D. Zermas, I. Izzat, and N. Papanikolopoulos, "Fast segmentation of 3D point clouds: A paradigm on LiDAR data for autonomous vehicle applications," in *IEEE International Conference on Robotics and Automation (ICRA)*, Singapore, May 2017, pp. 5067–5073.

Corentin Sanchez obtained his Master's degree in mechanical engineering from the Université de technologie de Compiègne (UTC), France, in 2017. He was awarded his Ph.D. degree by UTC in 2022. Since 2018 he has been a member of SIVALab, a laboratory run jointly by Renault, UTC and CNRS. His research interests cover self-driving vehicles, situation understanding, integrity and environment perception applied to autonomous navigation.

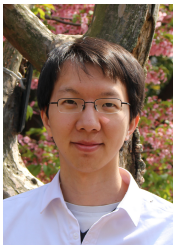

Philippe Xu received his M.S. degrees in computer science from the Ecole Normale Supérieure de Cachan, France, in 2011. He received his Ph.D. degree from the Université de Technologie de Compiègne (UTC), France, in 2014. Since 2015 he has been an associate professor in the Computer Science department of UTC and is carrying out his research in Heudiasyc UMR 7253 (UTC/CNRS). Since 2017 he has also been a member of SIVALab. His research interests cover information fusion, computer vision and machine learning applied to localization and perception for autonomous vehicles.

Philippe Bonnifait (Member, IEEE) received the Ph.D. degree in automatic control and computer science from the Ecole Centrale de Nantes, France, in 1997. He is currently a Professor with the Computer Science and Engineering Department, Université de Technologie de Compiègne, France. Since 1998 he has been part of Heudiasyc UMR 7253, a joint UTC-CNRS research laboratory. His research interests include intelligent vehicles navigation, in particular localization, mapping and perception of the environment using multi-sensor data fusion.

Alexandre Armand received his Ph.D. degree in computer science and robotics from ENSTA Paristech, France, in 2016. His research was done within the ADAS department at Renault, focusing on risk assessment. He then joined Renault's research division to work on autonomous driving technologies, with a particular interest in world modeling and situation understanding.